

Communication

Gold Nanorod Translocations and Charge Measurement through Solid-State Nanopores

Kimberly Venta, Mehdi B Zanjani, Xingchen Ye, Gopinath Danda,
Christopher B. Murray, Jennifer R. Lukes, and Marija Drndic

Nano Lett., Just Accepted Manuscript • DOI: 10.1021/nl502448s • Publication Date (Web): 05 Aug 2014

Downloaded from <http://pubs.acs.org> on August 5, 2014

Just Accepted

"Just Accepted" manuscripts have been peer-reviewed and accepted for publication. They are posted online prior to technical editing, formatting for publication and author proofing. The American Chemical Society provides "Just Accepted" as a free service to the research community to expedite the dissemination of scientific material as soon as possible after acceptance. "Just Accepted" manuscripts appear in full in PDF format accompanied by an HTML abstract. "Just Accepted" manuscripts have been fully peer reviewed, but should not be considered the official version of record. They are accessible to all readers and citable by the Digital Object Identifier (DOI®). "Just Accepted" is an optional service offered to authors. Therefore, the "Just Accepted" Web site may not include all articles that will be published in the journal. After a manuscript is technically edited and formatted, it will be removed from the "Just Accepted" Web site and published as an ASAP article. Note that technical editing may introduce minor changes to the manuscript text and/or graphics which could affect content, and all legal disclaimers and ethical guidelines that apply to the journal pertain. ACS cannot be held responsible for errors or consequences arising from the use of information contained in these "Just Accepted" manuscripts.



ACS Publications

High quality. High impact.

Nano Letters is published by the American Chemical Society. 1155 Sixteenth Street N.W., Washington, DC 20036

Published by American Chemical Society. Copyright © American Chemical Society. However, no copyright claim is made to original U.S. Government works, or works produced by employees of any Commonwealth realm Crown government in the course of their duties.

Gold Nanorod Translocations and Charge

Measurement through Solid-State Nanopores

15 Kimberly E. Venta,^{†,||} Mehdi B. Zanjani,^{‡,||} Xingchen Ye,[¶] Gopinath Danda,[§]

16
17 Christopher B. Murray,^{¶,§} Jennifer R. Lukes,[‡] and Marija Drndić^{*,†}

21 *Department of Physics and Astronomy, University of Pennsylvania, Philadelphia, PA*

22 *19104, USA, Department of Mechanical Engineering and Applied Mechanics, University of*

23 *Pennsylvania, Philadelphia, PA 19104, USA, Department of Chemistry, University of*

24 *Pennsylvania, Philadelphia, PA 19104, USA, and Department of Material Science and*

25 *Engineering, University of Pennsylvania, Philadelphia, PA 19104, USA*

32 E-mail: drndic@physics.upenn.edu

51 *To whom correspondence should be addressed

52 [†]Department of Physics and Astronomy, University of Pennsylvania, Philadelphia, PA 19104, USA

53 [‡]Department of Mechanical Engineering and Applied Mechanics, University of Pennsylvania, Philadelphia, PA 19104, USA

54 [¶]Department of Chemistry, University of Pennsylvania, Philadelphia, PA 19104, USA

55 [§]Department of Material Science and Engineering, University of Pennsylvania, Philadelphia, PA 19104, USA

56 ^{||}These authors contributed equally to this work.

Abstract

We study translocations of gold nanoparticles and nanorods through silicon nitride nanopores and present a method for determining the surface charge of nanorods from the magnitude of the ionic current change as nanorods pass through the pore. Positively-charged nanorods and spherical nanoparticles with average diameters 10 nm and average nanorod lengths between 44 and 65 nm were translocated through 40 nm thick nanopores with diameters between 19 and 27 nm in 1, 10, or 100 mM KCl solutions. Nanorod passage through the nanopores decreases ion current in larger diameter pores, as in the case of typical Coulter counters, but it increases ion current in smaller diameter nanopores, likely because of the interaction of the nanopore's and nanoparticle's double layers. The presented method predicts a surface charge of 26 mC/m^2 for 44 nm long gold nanorods and 18 mC/m^2 for 65 nm long gold nanorods and facilitates future studies of ligand coverage and surface charge effects in anisotropic particles.

KEYWORDS: Nanorods, Nanopores, Translocation, Surface Charge Density

Nanopores have found wide use for a variety of single-molecule studies¹⁻¹², including miRNA detection,¹³ discrimination between nucleic acid classes,^{13,14} detection of DNA binding,¹⁵ measurements of molecular forces,^{16,17} and anthrax toxin detection.¹⁸ The translocation properties of stiff, rod-shaped viruses has also been recently studied.¹⁹ Although their primary application has been towards next-generation DNA sequencing,¹² nanopores have previously been used for studies involving nanoparticles. Nanopores have found use to create and trap nanoparticles,²⁰ form nanoelectrodes,²¹ study single-walled nanotubes attached to single-stranded DNA,²² detect^{23,24} and separate²⁵ spherical gold nanoparticles, create nanoparticles²⁰ and nanorods,²⁶ and study colloids.²⁷ Carbon nanotube Coulter counters have previously been suggested as a method of characterizing spherical nanoparticle surface charge,^{28,29} microfluidics have been used to measure spherical nanoparticle size distributions,³⁰ and larger pores have been used to measure the zeta potential of polystyrene beads.³¹

In this paper, we demonstrate the use of nanopores for detection of charged nanorods (NR) and develop a method to measure their surface charge. The measurement of the charge of anisotropic nanoparticles is particularly challenging. Typically, the nanoparticle charge is measured using electrophoretic light scattering (ELS) measurements.^{32,33} While the charge of spherical particles can be measured accurately, these measurements are inaccurate for non-spherical particles with $\kappa a > 1$, where κ is the inverse Debye length, and a is the particle size.

In a traditional ELS measurement, particles are suspended in solution and a potential is applied across the solution. By measuring the Doppler shift of a reference laser passing through the suspension of particles as they are pulled through the solution, the particle mobility is extracted. This mobility can be used in combination with one of two approximations to calculate the surface potential. For the case where $\kappa a > 1$, where κ is the inverse Debye length and a is the particle size, the Hückel approximation is used.³⁴ The derivation of the Hückel approximation requires the formula for Stokes drag,³⁴ which is essentially derived

from an approximate analytical solution that exists only for spherical particles.³⁵ These approximate solutions, however, are not valid for nanorods. Once the surface potential is obtained, the Grahame equation³⁴ can be used to find the surface charge density:

$$\sigma = \frac{2\epsilon_r \epsilon_0 kT}{ze\lambda_d} \sinh\left(\frac{ze\psi_0}{2kT}\right) \quad (1)$$

Where σ is the surface charge density, ϵ_r is the relative permittivity of water, ϵ_0 is the vacuum permittivity, k is the Boltzmann constant, T is temperature, e is the elementary charge, z is the electrolyte valence, λ_d is the Debye length of solution, and ψ_0 is the surface potential.

Using nanopores we overcome this challenge. We present a method to characterize anisotropic particle charge. Our method proceeds in two steps. First, we measure the translocation of nanorods through a nanopore of known dimensions. We then use the information about the ionic current change to simulate the nanorods' translocation assuming a given surface charge. By iteratively altering the assumed surface charge until the simulations match the experimental results, we determine the nanorod surface charge. We first validate our model by translocating spherical gold nanoparticles of known charge, measured with ELS.

We demonstrate this technique on ~10-nm-diameter gold NRs using silicon nitride nanopores. The data are gathered in bulk quantities (most data sets in this paper contain over 500 events), but with information recorded on individual nanorods one at a time.

A schematic of the nanopore experimental design is shown in Fig. 1. A nanometer-sized pore in a thin membrane is positioned to divide two chambers of ionic solution such that the only path from one chamber to the other is through the nanopore. An electrode is placed in each chamber and connected to an amplifier, and nanorods are added to one chamber. When a potential is applied across the nanopore, a steady current, or open pore current, is observed. The potential also serves to drive the charged nanorods through the pore. As the nanorods pass through the nanopore, or translocate, their presence alters the current density

1
2
3 inside the nanopore, and a current change is noted in the electrical readout (Fig. 2). If the
4 presence of the nanorods decreases the current density through the nanopore, a decrease
5 is observed in the electrical readout, and if it increases the current density, an increase is
6 observed. We show from these events the charge on arbitrarily shaped nanoparticles can be
7 determined.
8
9

10 Silicon nitride membrane fabrication is described elsewhere.^{36,37} Briefly, suspended 40-
11 nm-thick silicon nitride membranes approximately 25 μm square are supported by 5 μm
12 of silicon dioxide (used for capacitance reduction) on 500 μm of n-type doped silicon. A
13 schematic cross-section of the completed membrane design is shown in Fig. 1 (a). Nanopores
14 are drilled in the silicon nitride membrane using the condensed beam of a JEOL 2010F
15 TEM.³⁸ The nanopores presented here have diameters in the range of 19 nm to 27 nm to
16 accommodate the NRs used. Fig. 1 (b) shows a TEM image of one such nanopore with a
17 diameter of 23 nm. To account for the fact that nanopores are not perfectly circular and
18 more accurately described by ellipses, nanopore area was measured from TEM images of the
19 nanopore, and the nanopore diameter was calculated from a circle of equivalent area. We
20 estimate the error in our nanopore diameter to be 0.5 nm due to measurement error. The
21 nanopore device is cleaned directly prior to testing in hot piranha solution for 10 minutes.
22 The nanopore is then sealed over an aperture in a polytetrafluoroethylene (PTFE) cell with
23 silicone elastomer, and positioned inside a PTFE channel, shown in Fig. 1(c). Salt solution
24 composed of 1 mM, 10 mM, or 100 mM KCl with EDTA at 1/1000 the KCl concentration
25 buffered to pH 8 using Tris-HCl at 1/100 the KCl concentration is injected into the cell and
26 channel. This low salt concentration is used to prevent NR aggregation, and NR aggregation
27 was checked using absorbance spectroscopy (see Supporting Information Fig. S2). Bias
28 potentials between 500 mV and 2000 mV are applied across the nanopore using Ag/AgCl
29 electrodes separated from the solution by a 1% agarose gel, and ionic current is monitored
30 as a function of time. Agarose gel is used to prevent any interaction of the nanorods or
31 nanorod coating with the electrodes.
32
33
34
35
36
37
38
39
40
41
42
43
44
45
46
47
48
49
50
51
52
53
54
55
56
57
58
59
60

Gold NR synthesis has been recently described elsewhere.³⁹ All NR samples used here are 10 ± 3 nm in diameter. The three NR samples used are either 65 ± 11 nm in length and 10 ± 2 nm in diameter, 45 ± 7 nm in length and 9 ± 2 nm in diameter, 44 ± 6 nm in length and 10 ± 2 nm in diameter, or spherical particles 12 ± 2 nm in diameter, as determined by analyzing a large number of particles from TEM images (see Supporting Information Fig. S1). A TEM image of a typical nanorod sample is shown in Fig. 1(d). NRs are colloidally stabilized with double layers of cetyltrimethylammonium bromide (CTAB), which gives the NRs a positive charge in solution and adds an additional 2 nm to all surfaces of the NR, making the gold nanorod-ligand system ~ 14 nm in effective diameter, as simulated below and illustrated in Fig. 1(e). The absorbance spectrum for nanorods in a range of KCl concentrations was checked, and for the salt concentrations presented here (100 mM KCl or less), the absorbance peaks were not found to broaden or red-shift, indicating the nanorods have negligible agglomeration at these salt concentrations (see Supporting Information Fig. S2).

Results and Discussion

Figure 2 shows one data set acquired during this experiment. Figure 2(a) shows segments of the current versus time trace acquired during the experiment. Voltage is applied to the top electrode (Fig. 1(c)) and measured at the bottom electrode, held at virtual ground. Before nanorods are added to the voltage-applying chamber, or when a negative voltage applied to the top electrode prevents the positively charged nanorod used here from translocating, no translocation events are seen (Fig. 2, top). When nanorods are added to the voltage-applying chamber and the correct positive voltage polarity is applied to the top electrode, nanorod translocations appear as spikes in the current versus time trace (Fig. 2, bottom). After the addition of nanoparticles, fluctuations in the baseline current are observed in some measurements. For example, Figure 2(c) shows baseline current fluctuations of \sim

1
2
3
4
5
6
7
8
9
10
11
12
13
14
15
16
17
18
19
20
21
22
23
24
25
26
27
28
29
30
31
32
33
34
35
36
37
38
39
40
41
42
43
44
45
46
47
48
49
50
51
52
53
54
55
56
57
58
59
60

0.1 nA at 1 V applied bias. Although these fluctuations may be due to the translocations of individual cetyltrimethylammonium molecules, which are large enough to modulate the nanopore current, but small enough, and translocate frequently enough, to avoid appearing as individual translocation events, we investigated the baseline noise dependence upon addition of CTAB molecules only and observed no noticeable increase in baseline noise (see Supporting Information Figure S4). However, baseline current fluctuations were observed to increase with applied voltage, and the voltage above which fluctuations became noticeable varied between nanopores. Although the origin of these fluctuations is unclear at present, evidence suggests it is not due to CTAB molecules in solution, but rather it may be related to inherent mechanisms of ion current flow through the nanopore at high applied bias. By plotting the change in conductance during an event (ΔG) versus the event duration, the distribution of event shapes becomes clear. Figures 2(b) and (c) show two more experiments using the nanopores pictured with a segment of the current versus time trace and their histogram distributions of event duration and ΔG .

32 We found that the percent change in the conductance, $\Delta G/G_0 = (G_0 - G_{event}) \times 100\% / G_0$,
33 where G_0 is the nanopore conductance without a nanoparticle present and G_{event} is the
34 nanopore conductance during nanoparticle translocation, decreases with increasing pore di-
35 ameter (see Fig. 3(a)), so that events increase the conductance in small diameter nanopores
36 (trace in Fig. 3(b)) and decrease the conductance in large diameter nanopores (trace in Fig.
37 3(c)). Figure 3(a) shows $\Delta G/G_0$ vs nanopore diameter for experiments using 100 mM KCl
38 in a range of nanopore diameters. If we use only a geometrical argument to understand
39 the dependence on $\Delta G/G_0$, where the nanopore functions as a resistor and a translocating
40 nanoparticle effectively reduces the resistor cross-sectional area (A), $G = \sigma A/l$, where σ is
41 the solution conductivity and l is the nanopore membrane thickness, then $\Delta G/G_0$ should
42 never be greater than 0 (shown as a dashed black line in Fig. 3(a)) because a resistor with
43 a smaller cross-sectional area should always have a lower conductivity. Further, from this
44 model, $\Delta G/G_0$ should asymptotically approach zero as the pore diameter grows because the
45

nanorod cross-sectional area accounts for a smaller fraction of the nanopore cross-sectional area as the nanopore diameter grows. This geometric model is plotted as a dashed blue line in Fig. 3(a). Instead, we observe that $\Delta G/G_0$ crosses over from positive to negative values as the nanopore diameter increases, corresponding to a transition from events that increase to events that decrease the current.

The regime of increased ionic current in smaller diameter nanopores during NR translocations is likely due to interaction between the Debye layers of the nanopore and nanorod. Our nanopores have been measured to have a negative surface charge similar to published values⁴⁰ due to hydroxyl groups that attach to the silicon during piranha treatment (See Supporting Information Fig. S3 for a measurement of pore surface charge), and the nanorods have a positive surface charge due to the dissociation of the Br⁻ ion from the CTAB coating. For small pores, the Debye layers of the nanorod and the nanopore overlap thereby increasing the net ion concentration inside the pore. If the increase in the total number of ions near the nanopore walls is greater than the number of ions that were blocked by the nanoparticle, a positive change in conductance is observed. Ionic mobility also plays a roll in the final nanopore conductance. Throughout a single experiment, we observe that either every event increases the conductance or every event decreases the conductance, but we never observe both increasing and decreasing events in the same experiment. Additionally, the same nanorod sample has shown events with increasing current in larger pores and events with decreasing current in smaller pores. This suggests that it is the nanopore diameter (relative to the constant nanorod diameter) and not the nanorod sample that is responsible for this phenomenon. Geometrically, in 100 mM KCl solution ($\lambda_d \approx 1$ nm), the electrical double layers should begin to overlap when the nanopore is ≤ 19 nm, and from Fig. 3(a), we see that the crossover between increasing and decreasing events occurs around 20 nm. A similar effect has been observed previously in DNA translocation experiments by altering the salt concentration⁴¹ or the pH,⁴² and both modifications will alter the size of the electrical double layers. Events that enhance conduction in silicon nitride nanopores were observed for

negatively charged gold nanoparticles²³ under similar conditions of low salt concentration and the ratio of nanoparticle to nanopore diameter of $\sim 0.5 - 0.8$, attributed to the interplay of surface charge values, salt concentration, and the ratio of nanopore to nanoparticle diameter. Event duration was also analyzed. As expected, longer NRs had longer translocation times (see Supporting Information Fig. S4). To elaborate on this point we consider a model that takes into account the nanopore blockade and the increase in the ion concentration due to the electric double layer effects. There are two significant contributions to ΔG . One due to the nanorod occluding the nanopore, which can be described as⁴¹

$$\Delta G_1 = -\frac{\pi}{4L_{pore}} d_{NR}^2 (\mu_{K^+} + \mu_{Cl^-}) N_a C_0 e \quad (2)$$

where N_a and e are the Avogadro Number and electron charge respectively. Here C_0 is the initial ion concentration in the solution. The other contribution, as shown in Fig. 3(d), comes from the ion concentration increase (ΔC) due to double layer effects

$$\Delta G_2 = +\frac{\pi}{4L_{pore}} (d_{pore}^2 - d_{NR}^2) (\mu_{K^+} + \mu_{Cl^-}) N_a \Delta C e \quad (3)$$

This results in $\frac{\Delta G}{G_0} = \frac{\Delta G_1 + \Delta G_2}{G_0} = \frac{\Delta C}{C_0} \left(1 - \frac{d_{NR}^2}{d_{pore}^2}\right) - \frac{d_{NR}^2}{d_{pore}^2}$; an average $\Delta G/G_0$ around 20% as observed in our measurements, would correspond in this model to an increase in ion concentration of about $\Delta C = 0.76C_0$ for a 19.5 nm diameter pore and a 11 nm diameter rod. This possibility is supported by Monte Carlo simulations of electrical double-layer formation inside nanopores⁴³ showing increases in ion concentration inside the nanopore, even as large as $\Delta C = 5C_0$. An increase in concentration is expected when the electric double layers play a significant role, which is the case for smaller nanopore diameters. The value of ΔC will in general depend on the specific nanopore and would be different for different nanopore sizes. Motivated by our work, future efforts may include a rigorous modeling of the overlapping double layers and their effect on ion transport inside nanopores.

Sample simulation results for spherical nanoparticles and nanorods are shown in Figures.

4(a) and 4(b). To validate our method for measuring anisotropic nanoparticle surface charge,
we first tested the method with spherical nanoparticles. The change in ionic current during
nanoparticle translocation is defined as ΔI . Experimentally, quoted ΔI values were found by
fitting a histogram of ΔI for hundreds of translocation events to a Gaussian distribution. To
compare simulation to experiment, finite element modeling was used to obtain a theoretical
prediction (ΔI_{th}). This value was then compared to the mean of the measured current
distribution (ΔI_{meas}). For the translocation of spherical nanoparticles through nanopores,
the nanoparticle surface charge density and all other required input parameters are known.
Here we focus only on systems with larger diameter pores that can be modeled as resistors
and in which the nanoparticle passage causes a decrease in ionic current. We used a finite
element model to calculate the electric current inside the pore (see Methods). In Fig. 4(a),
we have shown the electric potential profile obtained inside the pore in the presence of a
spherical nanoparticle of diameter 11 nm. As shown in Fig. 4 (c), at 2000 mV, for a 21
nm pore with 100 mM KCl and a translocating 11 nm spherical nanoparticle, the finite
element model predicts a value of $\Delta I_{th} = 1.0$ nA where the experimental results reveal
an value of $\Delta I_{meas} = 0.7 \pm 0.5$ nA. Therefore, the simulation result lies in between the
experimental measurement limits and we observe a good agreement between the simulation
and the experiment.

For nanorods, we can use the finite element model to estimate the nanorod surface charge
density σ_{rod} based on the experimental result for the current change (ΔI_{meas}) during nanorod
translocation. Since the only unknown parameter is the nanorod surface charge density,
choosing a specific value for σ_{rod} will result in a corresponding ΔI_{th} obtained from the
model. Therefore, through trial and error, i.e. by choosing different values for σ_{rod} as an
input parameter and calculating the corresponding ΔI_{th} from the finite element model, a
surface charge density that results in a ΔI_{th} matching with experimental data (ΔI_{meas}) can
be found. The trial and error was started from a surface charge density value of 10 mC/m²,
around that of the spherical nanoparticles, with steps of 2 mC/m² until a desirable value

for ΔI_{th} is obtained. The iteration is performed for both the upper and lower limits of ΔI_{meas} obtained from the experiments. The same procedure is repeated for translocation events of nanorods of two different lengths, 44 nm and 65 nm, inside a 19 nm pore. Based on these iterations, we obtained average values of $26 \pm 10 \text{ mC/m}^2$ and $18 \pm 9 \text{ mC/m}^2$ for the nanorod surface charge densities respectively. The average value of the surface charge density obtained here is larger than that of the spherical nanoparticles (14 mC/m^2). The surface charge density is usually proportional to the surface ligand coverage of the particles which typically scales with the surface to volume ratio.⁴⁴ This ratio is smaller for spherical shapes compared to cylinders, and thus we would expect lower ligand surface coverage for the spherical nanoparticles. For nanorods of different lengths but the same diameter, the surface to volume ratio is smaller for longer nanorods, consistent with surface charge densities that we obtained.

Using numerical simulations along with experimental data provides a promising method for characterizing and measuring unknown properties of nanoparticles of different shapes. The numerical method used here has also been used and validated for DNA translocation inside solid-state nanopores.⁴⁵ Compared to the ELS measurement, the numerical solution of the coupled Navier-Stokes and Maxwell equations in our method is more accurate than simple approximations assumed for spherical particles. At the same time, our method has the advantage that it can be generalized for particles with different shapes and geometries. Some typical limitations include the errors associated with the experimental measurements as well as the inaccuracies within the framework of continuum models, specially with regards to molecular level details for smaller nanopores, which are also common in other continuum level models such as the ones used with ELS measurements.

Conclusion

In this work, we demonstrated an original method for characterizing the surface charge on gold nanorods due to charged ligands. The method works by first measuring the current change and event duration during nanorod transit, then iteratively adjusting the surface charge value of the nanorod in simulations of translocations until the simulation matches the experiment. We first validated our method by measuring the surface charge on spherical nanoparticles and comparing it to values obtained by ELS, and found the numbers to be in good agreement. We found that in some experiments, translocation events increased the nanopore current while in others events decreased the current, for smaller and larger diameter nanopores, respectively. We surmise that this transition from positive to negative current change is due to the onset of interactions between the Debye layers of the nanoparticle and nanopore at low salt concentrations for nanopore diameters comparable to the nanoparticle size. While our model describes well the regime of $\Delta G/G_0 < 0$ in larger diameter nanopores, future work should include more detailed simulations to quantitatively explain the observed crossover of $\Delta G/G_0$ from positive to negative values as the nanopore diameter increases. We anticipate that future studies will make use of this new characterization method in experiments on charged nanorods.

Materials and Methods

Either a VC100 low-noise patch-clamp amplifier (Chimera Instruments) or an Axopatch 200B (Molecular Devices) was used to measure the current through the nanopore and apply a bias voltage. When the Chimera was used, data were sampled at 6 MHz bandwidth, and a fourth-order low-pass Bessel filter was applied at 1 MHz. All data were digitally filtered with a low-pass cutoff of 10 kHz and a sampling rate of either 50 or 100 kS/s. Custom Python software defines events as a percent change in the current relative to the standard deviation of the moving average open pore conductance. For analysis purposes, we consider

an event to end when the conductance value returns to within one standard deviation of its previous open pore conductance value. All current versus time trace displayed in this paper are displayed with the filtering settings with which they were analyzed.

Surface charge density values were extracted from zeta potential measurements. For nanorods, this value is an estimation due to violating the spherical particle assumption. The values extracted from these results were 10 mC/m^2 for the 65 nm long nanorods and 9 mC/m^2 for the 44 nm long nanorods. For spherical nanoparticles, this value represents a more accurate measurement of surface charge density. For the spherical nanoparticles used here, a value of 14 mC/m^2 was obtained.

Atomistic level models have been previously used to study the solid-state nanopores⁴⁶ as well as different properties of nanoparticles capped with organic ligands.^{47–51} Due to the computational limitations, these models prove to be useful for small sized systems with pores and nanoparticles of diameters below 5 nm. For larger systems, similar to the ones we study here, the kinetics of particle translocation through nanopores can be studied using continuum models. In the numerical simulations we used the finite element method to solve the coupled Navier-Stokes, Maxwell, and the Drift-Diffusion equations using COMSOL Multiphysics. For spherical nanoparticles we used an average diameter of 11 nm for the particle and 21 nm for the pore. For 100 mM KCl, we use values of $\mu_{K^+} = 6.10 \times 10^{-8} \text{ m}^2/\text{V s}$ and $\mu_{Cl^-} = 6.36 \times 10^{-8} \text{ m}^2/\text{V s}$ for the mobilities of of electrolyte⁴⁵ and a value of $\sigma = -23 \text{ mC/m}^2$ for the nanopore surface charge density (see Supporting Information Fig. S3). For nanorods, we consider a pore diameter of 19 nm, an average diameter of 11 nm for nanorods with rod length of 44 nm with voltage 1 V and another rod of length 65 nm with voltage 0.5 V.

Acknowledgement

This work was supported by the NSF MRSEC grant DMR-1120901. This material is based upon work supported by the National Science Foundation Graduate Research Fellowship (K.V.) under Grant No. DGE-0822. Any opinions, findings, and conclusions or recommen-

dations expressed in this material are those of the authors and do not necessarily reflect the views of the National Science Foundation. We gratefully acknowledge use of the TEM in the NSF-MRSEC electron microscopy facility.

Supporting Information Available

Histograms of nanoparticle and nanorod dimensions, absorbance spectrum of nanorods at varying salt concentrations, measurement of nanopore surface charge, event duration as a function of nanorod length, control experiment that CTAB micelles do not contribute to event count, and control experiment of CTAB's current contribution. This material is available free of charge via the Internet at <http://pubs.acs.org/>.

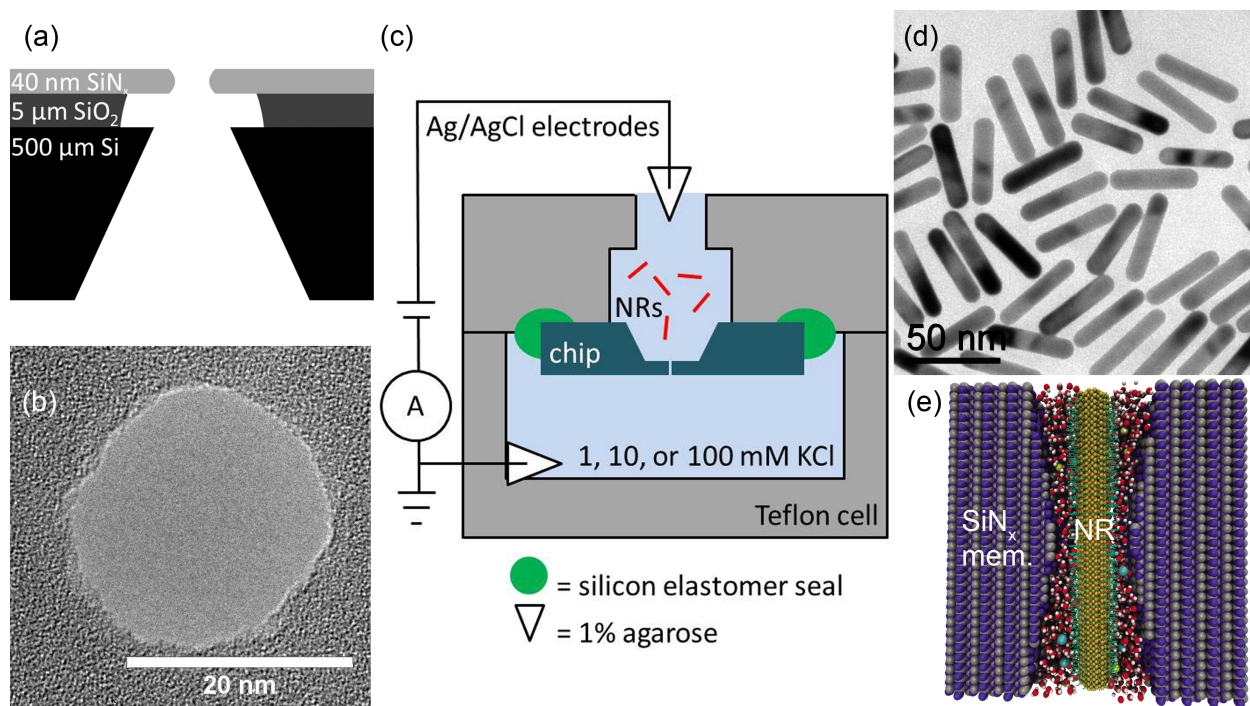


Figure 1: (a) Nanopore structure (not to scale). The nanopore is created in a 40-nm-thick silicon nitride membrane, as demonstrated in the TEM image. The silicon nitride membrane is supported by 5 μm of silicon dioxide for noise reduction, on a 500 μm silicon wafer. (b) TEM image of a nanopore. The nanopore shown is 23 nm in diameter. (c) Experimental design. The nanopore is placed to divide two chambers of KCl solution. A voltage bias is applied between the chambers, and nanorods are introduced to the chamber at higher bias. The nanorods are drawn through the nanopore by the potential bias. (d) Nanorod characterization. Nanorod samples ranged in length between 44 and 65 nm. The nanorods pictured are 10 nm in diameter and 44 nm long. (e) Demonstration of the nanorod-nanopore system. A nanorod capped with cetyltrimethylammonium bromide molecules inside a silicon nitride nanopore is illustrated with a 20 nm diameter nanopore and a 11 nm diameter nanorod. The silicon nitride pore is presented in purple and grey. In the center, the gold nanorod and the ligands are shown in yellow (NR) and green (ligands). In between the nanorod and the walls of the pore, water molecules and KCl ions are shown as red/white and green/yellow spheres, respectively.

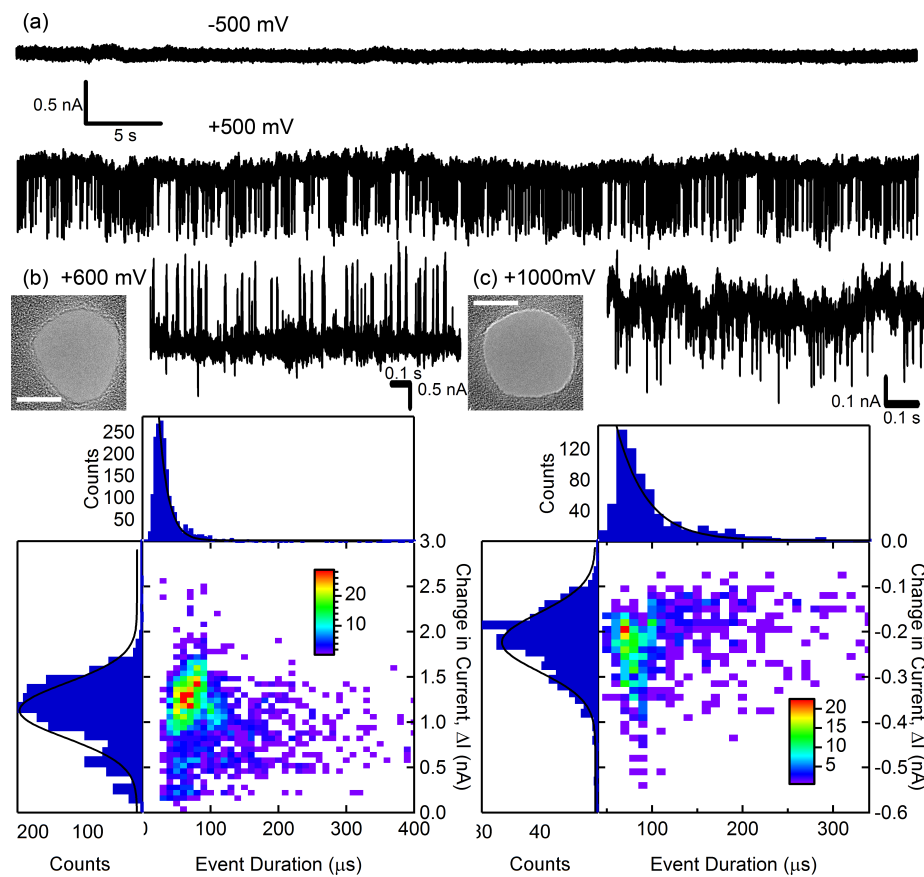


Figure 2: (a) A segment of a current trace for a nanorod experiment. This experiment used a 24 nm diameter nanopore with 65 nm long nanorods that were 10 nm in diameter. The data were taken in 10 mM KCl solution. Before nanorods are added, or when the voltage polarity is switched, no translocation events are seen, demonstrated in the top trace taken at -500 mV . After nanorods are added, spikes are seen in the current versus time trace (bottom trace taken at $+500\text{ mV}$). These are translocation events. This is the only experiment taken on the Axopatch 200B. All other experiments were taken on the Chimera VC100. (b) The results of another nanorod translocation experiment. This experiment was performed at -600 mV applied bias and 100 mM KCl, with a 19.3 nm diameter nanopore and 45 nm long, 9 nm diameter nanorods. Although occasional downward spikes can be seen in the current vs time trace, these events are extremely rare compared to the frequency of upward spikes, and are attributed to noise in the system. (c) The results of a nanorod translocation experiment. This experiment was performed at 1 V applied bias and 1 mM KCl, with a 20.4 nm diameter nanopore and 45 nm long, 9 nm diameter nanorods. For (b) and (c), a segment of the raw current vs time trace is shown at the top alongside a TEM image of the nanopore used in the experiment. The scale bars in the TEM images are 10 nm. Below is plotted a 2D histogram of the change in current (ΔI) during an event versus the duration of the event. Along the sides are the corresponding 1D histograms. ΔI is fit to a gaussian function, and event duration is fit to an exponential function to determine the quoted values of ΔI and event duration.

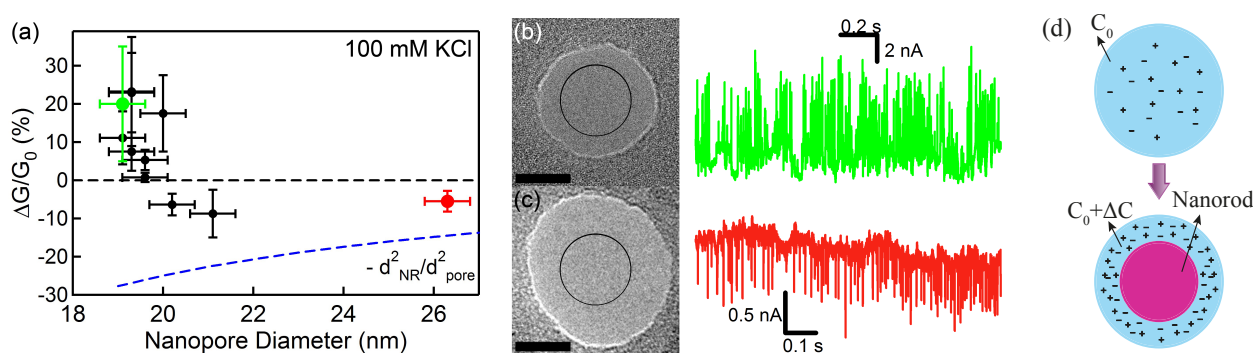


Figure 3: (a) Plot of the event percent change in the conductance during an event versus the nanopore diameter. Each marker represents a different current vs time trace collected. The nanoparticle lengths used in each experiment vary, but no trend was observed between nanoparticle length and $\Delta G/G_0$. The nanopore thickness (40 nm) and salt concentration (100 mM KCl) were held constant in all experiments shown. We found that the percent change in the conductance decreases as the nanopore diameter increases. $\Delta G/G_0$ error bars correspond to the standard deviation of histograms of the relative change of conductance during nanorod translocations. $\Delta G/G_0 = 0$ is marked with a dashed black line, and the theoretical curve based on geometric arguments ($-d_{NR}^2/d_{pore}^2$) is shown as a dashed blue line, where $d_{NR} = 10\text{ nm}$ is the nanorod diameter, and d_{pore} is the nanopore diameter. The data point shown in green corresponds to (b) the top nanopore and green current vs time trace. These data were taken with the 44 nm long nanorod sample at 1 V applied bias. Although the baseline fluctuates somewhat, all data sets including (b) were analyzed with a moving baseline, and events were defined as 5 standard deviations of the noise below the baseline. The data point shown in red in (a) corresponds to (c) the bottom nanopore and red current vs time trace. This data was taken with the spherical nanoparticle sample at 1V applied bias. The scale bars in the TEM images are 10 nm, and the black outline in the TEM images is a guide to the eye of the nanorod cross section, including the CTAB coating. (d) Schematic demonstration of the effect of electric double layer on ion concentration inside the nanopore.

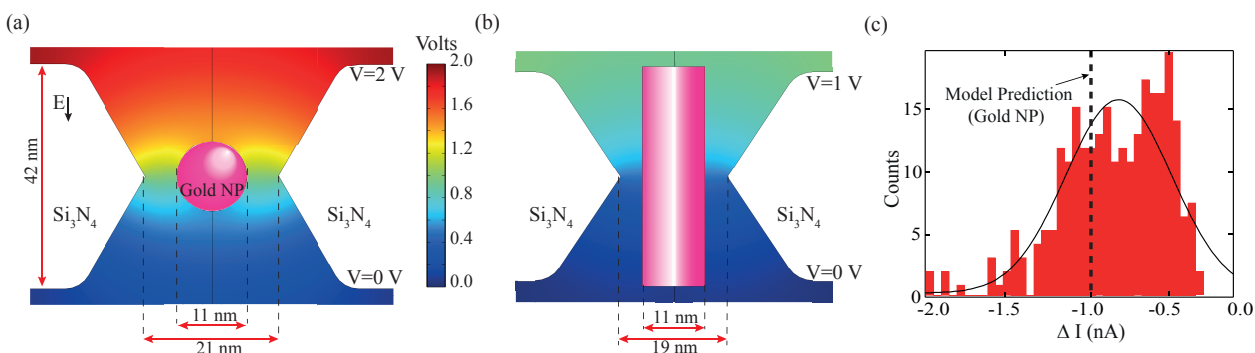


Figure 4: (a) Electric potential profile inside a nanopore during spherical nanoparticle translocation with voltage bias of 2 V, corresponding to ionic current changes shown in (c). The electric field vector points downwards in this picture. (b) Electric potential for nanorod translocation with voltage bias of 1 V, corresponding to ionic current data in Figs. 3 (b) and (c). (c) Change of ionic current, ΔI , during spherical nanoparticle translocation from experiments and simulation. The histogram of the current change is shown with the vertical dashed line representing the simulation result.

1
2
3
4

References

- 5
6 (1) Deamer, D.; Akeson, M. *Trends Biotechnol.* **2000**, *18*, 147–151.
7
8 (2) Deamer, D.; Branton, D. *Acc. Chem. Res.* **2002**, *35*, 817–825.
9
10 (3) Healy, K.; Schiedt, B.; Morrison, A. P. *Nanomedicine* **2007**, *2*, 875–897.
11
12 (4) Dekker, C. *Nat. Nanotechnol.* **2007**, *2*, 209–215.
13
14
15 (5) Branton, D. et al. *Nat. Biotechnol.* **2008**, *26*, 1146–1153.
16
17
18 (6) Kasianowicz, J. J.; Robertson, J. W. F.; Chan, E. R.; Reiner, J. E.; Stanford, V. M.
19
20
21 *Annu. Rev. Anal. Chem.* **2008**, *1*, 737–766.
22
23
24
25 (7) Howorka, S.; Siwy, Z. *Chem. Soc. Rev.* **2009**, *38*, 2360–2384.
26
27
28 (8) Keyser, U. F. *J. R. Soc. Interface* **2011**, *8*, 1369–1378.
29
30
31 (9) Venkatesan, B. M.; Bashir, R. *Nat. Nanotechnol.* **2011**, *6*, 615–624.
32
33
34 (10) Wanunu, M. *Phys. Life Rev.* **2012**, *9*, 125–158.
35
36
37 (11) Miles, B. N.; Ivanov, A. P.; Wilson, K. A.; Dogan, F.; Japrung, D.; Edel, J. B. *Chem.*
38
39
40 *Soc. Rev.* **2013**, *42*, 15–28.
41
42 (12) Kasianowicz, J.; Brandin, E.; Branton, D.; Deamer, D. *PNAS* **1996**, *93*, 13770–13773.
43
44
45 (13) Wanunu, M.; Dadash, T.; Ray, V.; Jin, J.; McReynolds, L.; Drndic, M. *Nat. Nanotechnol.*
46
47 **2010**, *5*, 807–814.
48
49
50 (14) Folgea, D.; Gershaw, M.; Ledden, B.; McNabb, D.; Golovchenko, J.; Li, J. *Nano Lett.*
51
52 **2005**, *5*, 1905–1909.
53
54
55 (15) Kowalczyk, S. W.; Hall, A. R.; Dekker, C. *Nano Lett.* **2010**, *10*, 324–328.
56
57
58
59
60

- (16) Keyser, U. F.; Koeleman, B. N.; Van Dorp, S.; Krapf, D.; Smeets, R. M. M.; Lemay, S. G.; Dekker, N. H.; Dekker, C. *Nat. Phys.* **2006**, *2*, 473–477.
- (17) Dudko, O. K.; Mathe, J.; Szabo, A.; Meller, A.; Hummer, G. *Biophys. J.* **2007**, *92*, 4188–4195.
- (18) Halverson, K.; Panchal, R.; Nguyen, T.; Gussio, R.; Little, S.; Misakian, M.; Bavari, S.; Kasianowicz, J. *J. Biol. Chem.* **2005**, *280*, 34056–34062.
- (19) McMullen, A.; de Hann, H. W.; Tang, J. X.; Stein, D. *Nat. Commun.* **2014**, *5*, 1–10.
- (20) Venta, K.; Wanunu, M.; Drndic, M. *Nano Lett.* **2013**, *13*, 423–429.
- (21) Krapf, D.; Wu, M.; Smeets, R.; Zandbergen, H.; Dekker, C.; Lemay, S. *Nano Lett.* **2006**, *6*, 105–109.
- (22) Hall, A. R.; Keegstra, J. M.; Duch, M. C.; Hersam, M. C.; Dekker, C. *Nano Lett.* **2011**, *11*, 2446–2450.
- (23) Goyal, G.; Freedman, K. J.; Kim, M. J. *Anal. Chem.* **2013**, *85*, 8180–8187.
- (24) Campos, E.; McVey, C. E.; Carney, R. P.; Stellacci, F.; Astier, Y.; Yates, J. *Anal. Chem.* **2013**, *85*, 10149–10158.
- (25) Prabhu, A. S.; Jubery, T. Z. N.; Freedman, K. J.; Mulero, R.; Dutta, P.; Kim, M. J. *J. Phys.-Condens. Matter* **2010**, *22*.
- (26) Sharabani, R.; Reuveni, S.; Noy, G.; Shapira, E.; Sadeh, S.; Selzer, Y. *Nano Lett.* **2008**, *8*, 1169–1173.
- (27) Bacri, L.; Oukhaled, A. G.; Schiedt, B.; Patriarche, G.; Bourhis, E.; Gierak, J.; Pelta, J.; Auvray, L. *J. Phys. Chem. B* **2011**, *115*, 2890–2898.
- (28) Ito, T.; Sun, L.; Henriquez, R.; Crooks, R. *Acc. Chem. Res.* **2004**, *37*, 937–945.

- 1
2
3 (29) Ito, T.; Sun, L.; Crooks, R. *Anal. Chem.* **2003**, *75*, 2399–2406.
4
5 (30) Fraikin, J.-L.; Teesalu, T.; McKenney, C. M.; Ruoslahti, E.; Cleland, A. N. *Nat. Nan-*
6
7 *otechnol.* **2011**, *6*, 308–313.
8
9
10 (31) Kozak, D.; Anderson, W.; Vogel, R.; Chen, S.; Antaw, F.; Trau, M. *ACS Nano* **2012**,
11
12 *6*, 6990–6997.
13
14
15 (32) Delgado, A. V.; Gonzalez-Caballero, F.; Hunter, R. J.; Koopal, L. K.; Lyklema, J.
16
17 *J. Colloid interf. Sci.* **2007**, *309*, 194–224, International Electrokinetics Conference
18
19 (Elkin), Nancy, FRANCE, JUN 25-29, 2006.
20
21
22
23 (33) Hunter, R. J. *Zeta potential in colloid science: principles and applications*; Academic
24
25 Press, 1981.
26
27
28 (34) Ohshima, H. *Theory of Colloid and Interfacial Electric Phenomena*; Academic Press,
29
30 2006.
31
32
33 (35) Batchelor, G. *An Introduction to Fluid Dynamics*; Cambridge University Press, 2000.
34
35
36 (36) Fischbein, M.; Drndic, M. *Appl. Phys. Lett.* **2006**, *88*.
37
38
39 (37) Healy, K.; Ray, V.; Willis, L. J.; Peterman, N.; Bartel, J.; Drndic, M. *Electrophoresis*
40
41 **2012**, *33*, 3488–3496.
42
43
44 (38) Storm, A.; Chen, J.; Ling, X.; Zandbergen, H.; Dekker, C. *Nat. Mater.* **2003**, *2*, 537–
45
46 540.
47
48
49 (39) Ye, X.; Jin, L.; Caglayan, H.; Chen, J.; Xing, G.; Zheng, C.; Doan-Nguyen, V.; Kang, Y.;
50
51 Engheta, N.; Kagan, C. R.; Murray, C. B. *ACS Nano* **2012**, *6*, 2804–2817.
52
53
54 (40) Sonnfeld, J. *Colloid Surface A* **1996**, *108*, 27–31.
55
56
57 (41) Smeets, R.; Keyser, U.; Krapf, D.; Wu, M.; Dekker, N.; Dekker, C. *Nano Lett.* **2006**,
58
59 *6*, 89–95.
60

- 1
2
3 (42) Firnkes, M.; Pedone, D.; Knezevic, J.; Doeblinger, M.; Rant, U. *Nano Lett.* **2010**, *10*,
4 2162–2167.
5
6
7 (43) Hou, C.-H.; Taboada-Serrano, P.; Yiaccoumi, S.; Tsouris, C. *J. Chem. Phys.* **2008**, *128*,
8 044705.
9
10
11 (44) Kalesky, R. J. B.; Shinoda, W.; Moore, P. B.; Nielsen, S. O. *Langmuir* **2009**, *25*,
12 1352–1359.
13
14
15 (45) Vlassarev, D. M.; Golovchenko, J. A. *Biophys. J.* **2012**, *103*, 352–356.
16
17
18 (46) Aksimentiev, A.; Heng, J. B.; Timp, G.; Schulten, K. *Biophys. J.* **2004**, *87*, 2086.
19
20
21 (47) Rabani, E. *J. Chem. Phys.* **2001**, *115*, 1493–1497.
22
23
24 (48) Kaushik, A. P.; Clancy, P. *J. Comput. Chem.* **2013**, *34*, 523.
25
26
27 (49) Zanjani, M. B.; Lukes, J. R. *J. Chem. Phys.* **2013**, *139*, 144702.
28
29
30 (50) Landman, U.; Luedtke, W. D. *R. Soc. Chem.* **2004**, *125*, 1–22.
31
32
33 (51) Zanjani, M. B.; Lukes, J. R. *J. Appl. Phys.* **2014**, *115*, 143515.
34
35
36
37
38
39
40
41
42
43
44
45
46
47
48
49
50
51
52
53
54
55
56
57
58
59
60

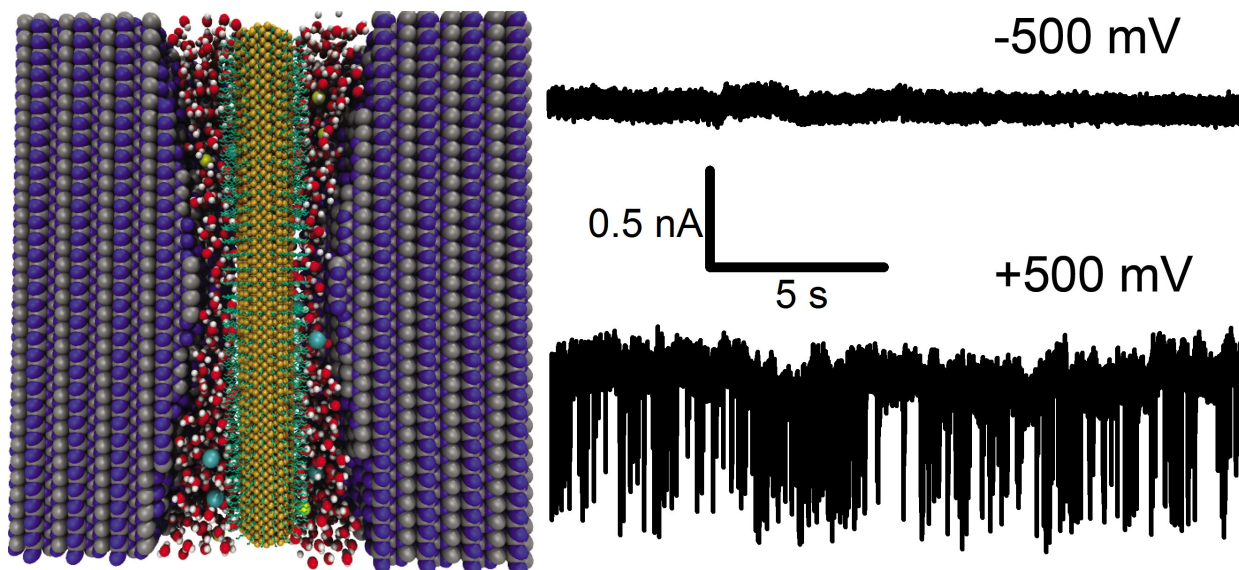


Figure 5: For TOC only